HiSST: 2nd International Conference on High-Speed Vehicle Science Technology
11–15 September 2022, Bruges, Belgium

Wall Pressure Stability and Cooling Efficiency Analysis in a Transpiration-Cooled Scramjet Model Combustor

Friedolin T. Strauss[1], Stephan General[2], Patrick A. Cragg[3], Stefan Schlechtriem[4]

Abstract

This publication presents the results of an ongoing investigation into transpiration cooling of scramjets at the German Aerospace Center (DLR). It summarizes the shock-boundary layer interaction results and the influence of this interaction on the systems' cooling efficiency and performance from more than 1000 hot run tests. Special focus is placed on the local static pressure distribution on the upper wall in the coolant wake region. Furthermore, different flow interaction phenomena were discovered and are thoroughly analyzed by the application of state of the art optical and non-intrusive measurement techniques like Background Oriented Schlieren (BOS) combined with pressure and temperature data analysis and correlations. The unique SBLI behavior of the coolant is addressed in this publication. Three different porous wall materials made of sintered stainless steel are compared and analyzed in terms of performance and sensitivity to shock-boundary layer interaction issues. It was found that the shock generator generates a stronger geometric contraction in the hot gas main flow if positioned at the downstream position. Thus, this position is more prone t generating shock trains and generates a stronger impact on the static wall pressure distribution in the coolant wake region. It is proven in this publication that the main drivers for influencing the static wall pressure distribution are the hot gas mass flow rate (stagnation pressure more important than stagnation temperature) and the impingement position of the shock generator's oblique shock. The static wall pressure distribution was found to be mostly independent of the changes in static wall temperature and in cooling efficiency. An outlook on the results of additional experiments using different types of porous media (e.g. ceramics) and improved measurement techniques with the same coolants is also presented. Further research requirements and subsequent changes in the test setup are discussed

Keywords: *Scramjet, Ground Testing, Transpiration Cooling, Thermodynamics, Gasdynamics*

Nomenclature

Latin
A – Area [m²]
F – Blowing Ratio [-]
$\dot{m}$ – Mass Flow Rate [kg/s]
T – Temperature [K]

Subscripts
c – Coolant
e – Nozzle Exit
g – Hot Gas

[1] *German Aerospace Center (DLR), D-74239 Hardthausen, Germany, Friedolin.Strauss@dlr.de*
[2] *German Aerospace Center (DLR), D-74239 Hardthausen, Germany, Stephan.General@dlr.de*
[3] *German Aerospace Center (DLR), D-74239 Hardthausen, Germany, Patrick.Cragg@dlr.de*
[4] *German Aerospace Center (DLR), D-74239 Hardthausen, Germany, Stefan.Schlechtriem@dlr.de*

1. Introduction

Internationally, research on sustainable and efficient alternatives to current aerospace propulsion systems has increased demand for replacement of toxic propellants and for the modernization of existing systems through greater efficiency. These drivers along with national security challenges have brought ramjets with supersonic combustion (scramjets) and other systems back into focus (see e.g. [1]-[3]). The main challenges of high-speed air-breathing propulsion systems like scramjets are short fuel residence times, controlled mixing and combustion, and efficient /sufficient cooling of the engine's components exposed to very high heat loads (up to 5 MW / m² with wall temperatures of 3000 K at flight velocities of Mach 8, see [4], [5]). Transpiration cooling is a promising approach to mitigate these high heat loads. In this cooling method, the coolant flows through a porous wall prior to entering the engine's main hot gas flow. Penetration of the main hot gas flow by the coolant can be improved by a phase change from liquid to gas [6]. By using transpiration cooling, a homogeneous and protective coolant layer of the engine wall could be achieved, protecting the areas with high thermal loads while keeping the engine structure at moderate temperatures. The introduction of a coolant secondary flow into the main hot gas flow can lead to phenomena like thermal choking, shock-boundary layer interaction (SBLI) and boundary layer combustion, and are not yet fully understood. A thorough literature analysis of comparable experiments with similar porous materials can be found in Ref. [7]. For detailed literature information on the optical measurement techniques, refer to Ref. [8].

This publication presents results of the ongoing investigation of transpiration cooling of scramjets conducted at the German Aerospace Center (DLR). It summarizes selected shock-boundary layer interaction results from more than 1000 hot run tests and the influence of this interaction on the performance of the system. Special focus is placed on the local static pressure distribution in the coolant wake region on the combustion chamber's upper wall. Different flow interaction phenomena were discovered and are thoroughly analyzed by the application of state of the art optical and intrusive measurement techniques like Background Oriented Schlieren (BOS) combined with pressure data analysis and correlation. The unique SBLI behavior of the coolants used is addressed in this publication. Three different porous wall materials are compared and analyzed in terms of performance and sensitivity to shock-boundary layer interaction issues. An outlook is presented on the results of additional experiments using different types of porous media (e.g. ceramics), different shock generator positions, and improved measurement techniques with the same coolants. Further research requirements and subsequent changes in the test setup are discussed.

2. Experimental Setup

The Institute of Space Propulsion of the German Aerospace Center (DLR), Lampoldshausen has developed and established a research test bench to investigate the applicability of transpiration cooling systems to scramjets and to examine the resulting phenomena in the supersonic flow [7], [9],[10], [11]-[15]. The test bench (see [9], [10] for details and performance) consists of a hydrogen / oxygen air vitiator (A, B, C in Fig. 1 and Fig. 2) with 11 hydrogen / oxygen burners that heat up the pressurized air fed through them. They can be interconnected in different burner patterns to adjust the mass flow, pressure, and temperature of the vitiated air as required.

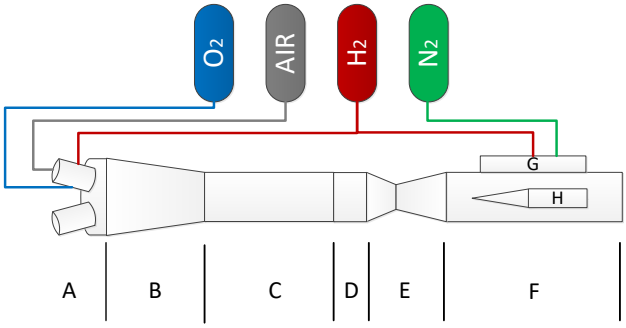

Fig 1. Test Bench Scheme

It is possible to reach stagnation temperatures up to 1500 K, stagnation pressures of 25 to 30 bars and mass flows of 5,0 kg /s maximum with the air vitiator. Connected to the air vitiator is a geometrical

transition section that converts the round cross-section (diameter 135 mm) into a rectangular cross-section (45 by 45 mm) with minimal influence on the boundary layer (D in Fig. 1).

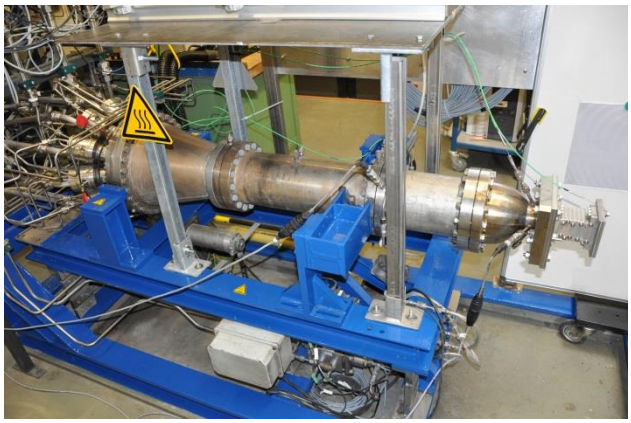

Fig 2. Air Vitiator

A Mach nozzle (E in Fig. 1) follows the transition section to accelerate the flow to a Mach number of 2.5, which is then connected to the test combustion chamber (F in Fig. 1 and Fig. 3). The versatile combustion chamber (length 300 mm) can accommodate an exchangeable wedge shaped strut (H in Fig. 1) to induce different shock patterns that interfere with the coolant boundary layer. This option was used in the shock-boundary layer interaction (SBLI) experiments at different lateral positions of the shock generator. The combustion chamber can be supplied by a plenum (G in Fig. 1) with different coolants and fuels, including gaseous nitrogen and gaseous hydrogen. The combustion chamber can be equipped with different porous wall segments with the dimensions of 130 x 30 mm and a thickness of 20 mm. They are made of high temperature resistant stainless steel and Inconel with different porosities or CMC ceramics.

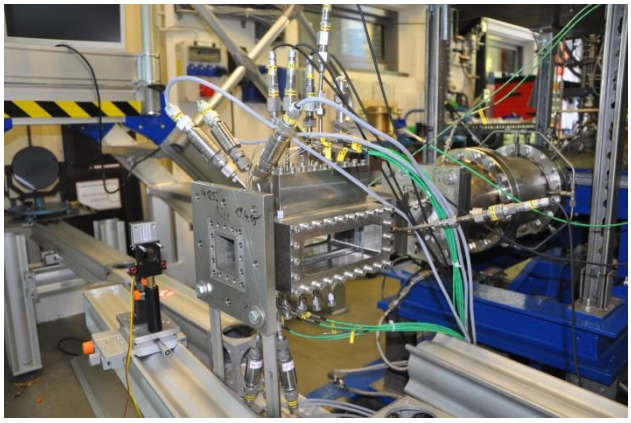

Fig 3. Ramjet / Scramjet Model Combustion Chamber

This makes it possible to investigate the influence of different porous wall materials with various technical specifications and diverse porosities on the cooling efficiency. Gaseous nitrogen and gaseous hydrogen were used during the test campaign as coolants with different plenum pressures. Two quartz glass windows provide optical access and allow the use of a z-type Schlieren system with a total optical length of 7 m for flow investigations [16]. For some of the test runs the z-type Schlieren system was replaced by a Background Oriented Schlieren (BOS) system [8], [17]. This system features detailed Schlieren imagery and was shown in the experiments to be less affected by changes in the refractive index of the quartz glass windows due to strong heating [8].

3. Experimental Methodology

In the interaction experiments, a half wedge located directly at the lower wall with a 9.3° half angle was used. This half wedge could be positioned vertically and laterally with a pressure tight positioning mechanism. For this publication one lateral position of the shock generator was investigated (177 mm from the scramjet model combustion chamber's intake plane). The boundary conditions provided by

the air vitiator for the experiments were a 900 K stagnation temperature at 10.0 and 15.0 bar stagnation pressures and a 1200 K stagnation temperature at 10.0 and 15.0 bar stagnation pressures. These boundary conditions yield four distinct hot gas mass flow rates. The boundary conditions provided by the air vitiator were very stable, especially in terms of reproducibility of the phenomena described below at the corresponding test points (see also [9]). For each air vitiator boundary condition four different coolant blowing ratios were investigated with constant pressures in the coolant plenum for every single blowing ratio and both coolants [7]. At each of the four different sets of boundary conditions provided by the air vitiator, three different testing configurations of the model combustion chamber were tested. The first configuration included a lateral optical access by quartz glass windows without shock generator. A measurement plate is also positioned on the bottom wall, which is equipped with additional pressure and temperature sensors. The second configuration included the shock generator instead of the bottom wall measurement plate. The third configuration included the shock generator and an additional lateral measurement plate instead of one of the windows (see [7] and [14] for details). Phenomena such as hot spots on the porous wall, inefficient cooling, shock boundary layer interaction (see Fig. 4) and SBLI induced coolant self-ignition were observed in the experiments (see also [7], [13]-[15]). With the BOS setup it is possible to analyze the development and the behavior of those phenomena. Additional hot runs were performed with a high-speed BOS system using a high-speed camera for the chamber flow path analysis and simultaneously a second high-speed camera for analysis of the exit flow pattern (e.g. to detect external hydrogen ignition and combustion). The optical data obtained by this approach can be correlated with the channel's pressure distribution in the coolant wake region. Thickening of the boundary layer / boundary layer separation was demonstrated e.g. while using hydrogen as coolant (see Fig. 4) by application of the BOS system. The development of shock trains forced by the introduction of a secondary coolant flow leads to an increased physical blockage up to the choking case.

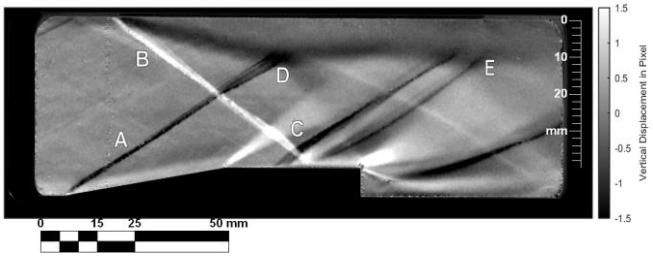

Fig 4. Shock-Boundary Layer Interaction (BOS Image), Shock Generator at 112 mm Position

Fig. 4 demonstrates a typical shock-boundary layer interaction (SBLI), in this case with the shock generator positioned at 112 mm from the inlet plane. A strong interaction of the shock ("A") generated by the shock generator, the shock generated by the coolant boundary layer ("B"), and the coolant film itself is visible. These interactions ("D" and "E") lead to a thickening of the coolant boundary layer and two separation bubbles on the porous wall segment. Despite this separation, it was found that the cooling efficiency downstream of the separation bubble is still sufficient. It was found that hydrogen provides a coolant boundary layer that is much more insensitive to shock-boundary layer interaction issues than a nitrogen coolant boundary layer. Hydrogen is a higher performing coolant that literally insulates the wall region from the hot gas region even at small blowing ratios. However, the introduction of a coolant secondary flow at high blowing ratios can lead to physical blockage of the combustion chamber and to a subsonic flow due to choking. Even without choking, the increased turning angle caused by the secondary flow can lead to pre-choking phenomena like fluctuating shock trains, increasing the mixing of hot gas with coolant. This mixing with hot gas main flow / ram air as oxidizer can lead to self-ignition of the hydrogen coolant triggered by shocks impinging the coolant boundary layer. See [18] for details on SBLI in transpiration cooling.

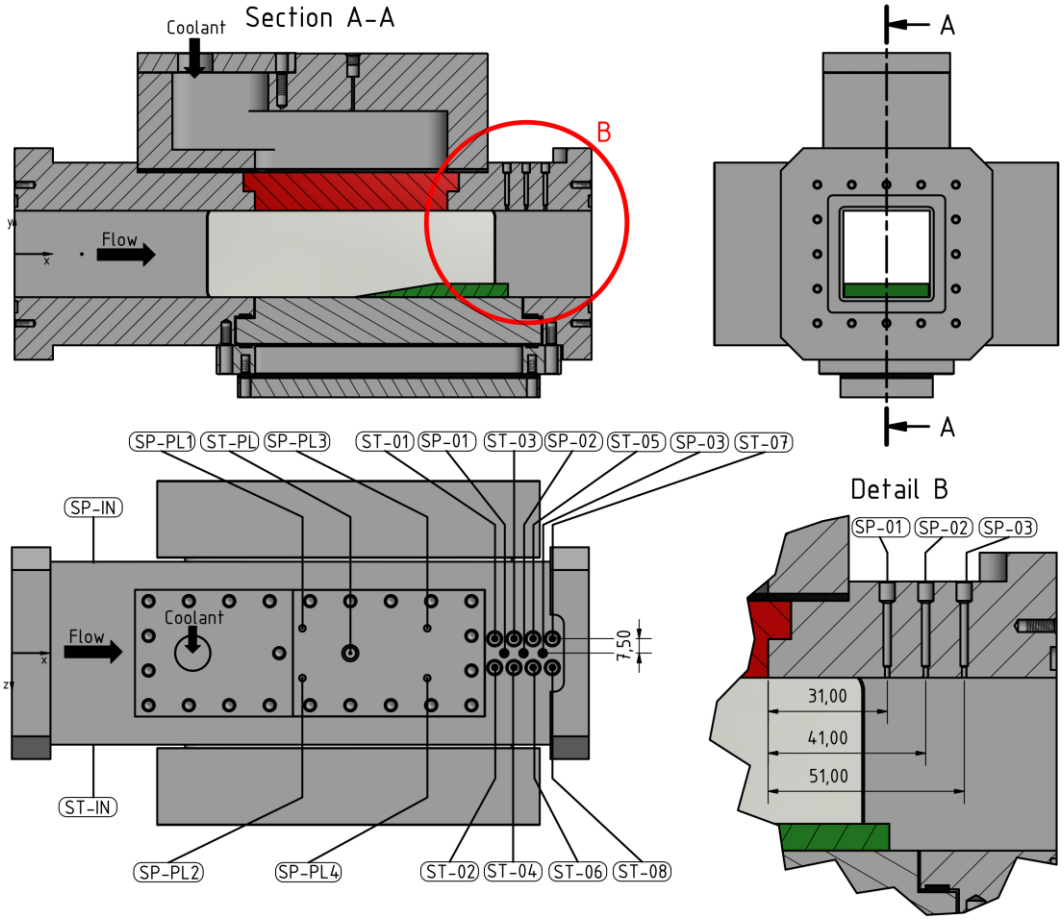

Fig 5. Sensor Positions for Wall Temperature and Static Wall Pressure in the Coolant Wake Region

The position of the shock generator and its induced oblique shock strongly affects the cooling efficiency. If the shock impinges more downstream it decreases the cooling efficiency (see [7] and [15]). Fig. 5 displays the positions of pressure and temperature sensors in the test configuration with lateral optical access and a shock generator position at 177 mm.

4. Results

Figures 6 to 17 compare the static wall pressure distributions in the wake region at sensors "SP-01" to "SP-03" (refer to Fig. 5 for their positions) for a shock generator position at 177 mm downstream of the combustion chamber's inlet plane. All figures refer to a hydrogen coolant only, since nitrogen has a stronger effect on the hot gas main flow which would cause a choking of the channel if the shock generator is positioned at 177 mm.

The corresponding wall temperature distribution graphs for all figures can be found in [15]. For Schlieren comparison of the flow path without a shock generator to a flow path with a shock generator in place and hydrogen coolant refer to [14]. For a flow path comparison between the two coolants, nitrogen and hydrogen, refer to [7], [12]. For better legibility, the analysis has been limited to a comparison between the uncooled and maximum cooled case at each boundary condition for each porous material used. BOS images are included in the graphs and visualize the flow field for each maximum blowing ratio. However, these images serve only general informational purposes. For a detailed Schlieren flow field analysis at different boundary conditions refer to Ref. [7, 12, 14].

The blowing ratio F is defined according to Eq. 1 and [5].

$$F = \frac{\dot{m}_c A_g}{\dot{m}_g A_c} \tag{1}$$

The hot gas main mass flow $\dot{m}_g$ in Eq. 1 is determined through measurements at the air vitiator. The coolant mass flow $\dot{m}_c$ in Eq. 1 is determined by the Coriolis coolant mass flow meter [9], [10]. A_g indicates the cross section area of the channel and A_c is the area of the porous wall segment.

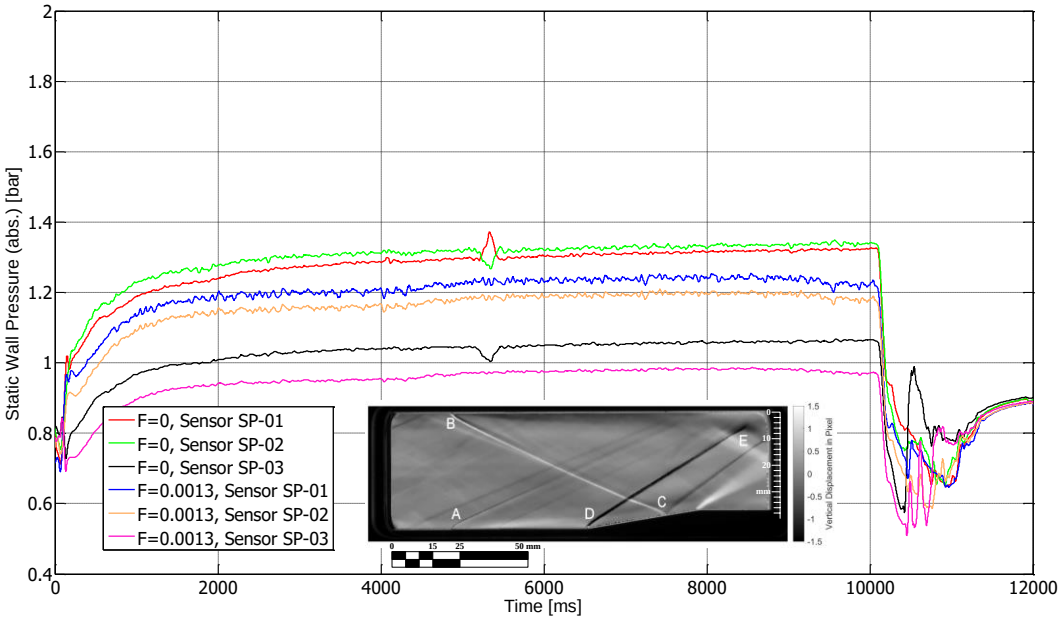

Fig 6. Static Wall Pressures in the Coolant Wake Region, 900 K, 10 bar Stagnation Values, Hydrogen, Shock Generator Position 177 mm, Sika-IL 1.

Figure 6 shows the static wall pressure distribution for Sika-IL 1 at a 900 K and 10 bar stagnation condition. Due to the position of the shock impingement point and the impingement of the expansion fan created by the shock generator, sensors "SP-01" and "SP-02" show similar readings, whereas sensor "SP-03" shows a lower value. This indicates an acceleration event (e.g. by the impinging expansion fan) between sensors "SP-02" and "SP-03". If a hydrogen coolant boundary layer is introduced at a blowing ratio of F=0.13 %, the absolute values are reduced due to an acceleration of the flow most likely caused by the resulting contraction in the effective cross section area. However, the differences between the sensors persist. Compared to the flow field with the shock generator at 112 mm (see [19]), the absolute values are 0.3 to 0.6 bar higher and additionally the flow reacts more strongly to the introduction of a coolant secondary flow than in the 112 mm case.

Figure 7 displays the static wall pressure distribution in the wake region for the same boundary conditions as Fig. 6, but with Sika-IL 20 installed, resulting in a higher maximum blowing ratio of F=0.93%. Compared to Fig. 6 the uncooled case shows a similar pressure distribution as expected. However, if a coolant secondary flow is introduced, the flow pattern responds with the development of a shock train and a thick coolant boundary layer (refer to BOS image in Fig. 7 and [7]). In contrast to this, the shock generator does not generate a shock train pattern at the same boundary conditions as at its 112 mm position (compare with [19]). The generated coolant boundary layer affects the static wall pressure more strongly in the 177 mm case than in the 112 mm case. In Ref [19] the pressure rise at sensor "SP-03" between the uncooled and cooled case is 0.1 bar, whereas in Fig. 7 the difference is approximately 0.4 bar.

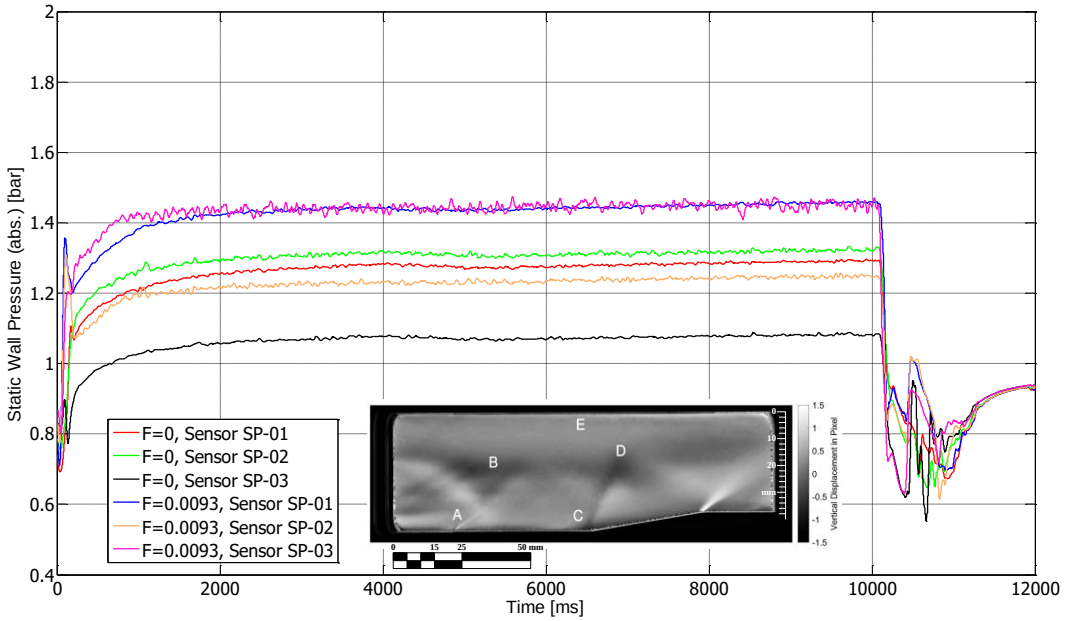

Fig 7. Static Wall Pressures in the Coolant Wake Region, 900 K, 10 bar Stagnation Values, Hydrogen, Shock Generator Position 177 mm, Sika-IL 20.

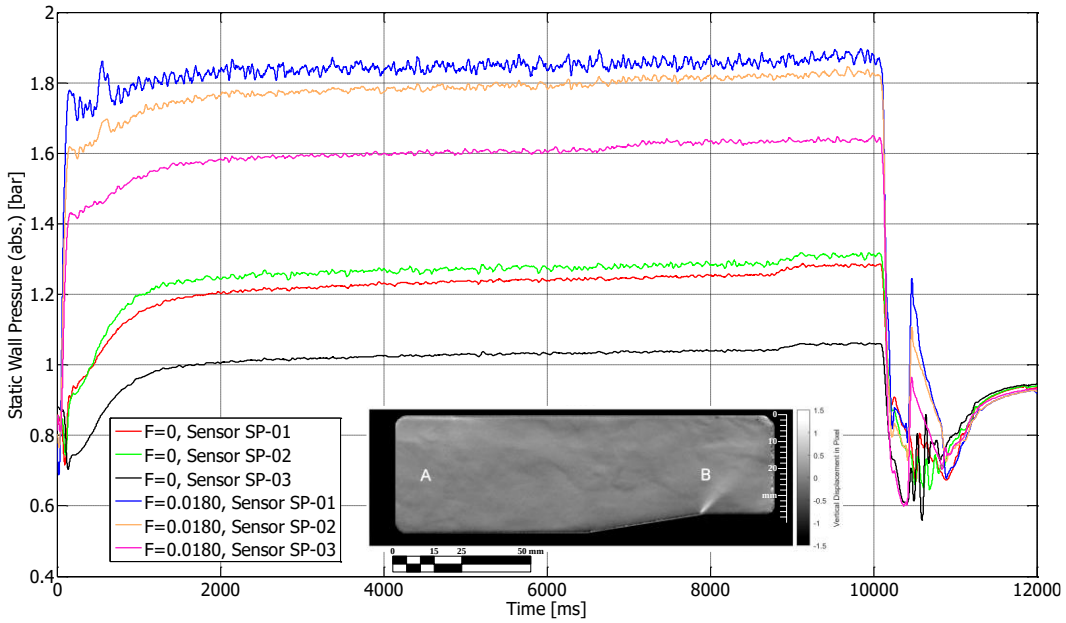

Fig 8. Static Wall Pressures in the Coolant Wake Region, 900 K, 10 bar Stagnation Values, Hydrogen, Shock Generator Position 177 mm, Sika-R 150.

Figure 8 shows the static wall pressure distribution at a 900 K, 10 bar stagnation condition for the coarsest porous material Sika-R 150. The pressure distribution without cooling is as in Fig. 6 and 7. However, the high blowing ratio of F=1.8 % induces the flow to first develop a strong shock train system and ultimately choke the flow field to subsonic speeds. This is indicated by the strong pressure rise for all sensors from "SP-01" to "SP-03". The absolute value rises, but the relative difference between the sensors stays the same, which indicated a fully choked flow (see also [7] for details on the buildup of this phenomenon). At a shock generator position of 112 mm, the maximum static wall pressure value is 0.6 bar lower and the flow still shows a non-choked state with a shock train.

Figure 9 shows the static wall pressure distribution for a 900 K, 15 bar stagnation condition with Sika-IL 1. Compared to the 112 mm position of the shock generator, the maximum static pressure in the uncooled case is 0.6 to 1.0 bar higher (depending on the sensor). The differences between the three pressure sensors "SP-01" to "SP-03" are slightly higher than in the 900 K, 10 bar case. Additionally the coolant secondary flow affects the wall pressure distribution in a similar manner to the 900 K, 10 bar

case (see Fig. 6). The effect of the coolant introduction is much stronger at the same blowing ratio and the same stagnation values than at the 112 mm shock generator position (compare to [19]).

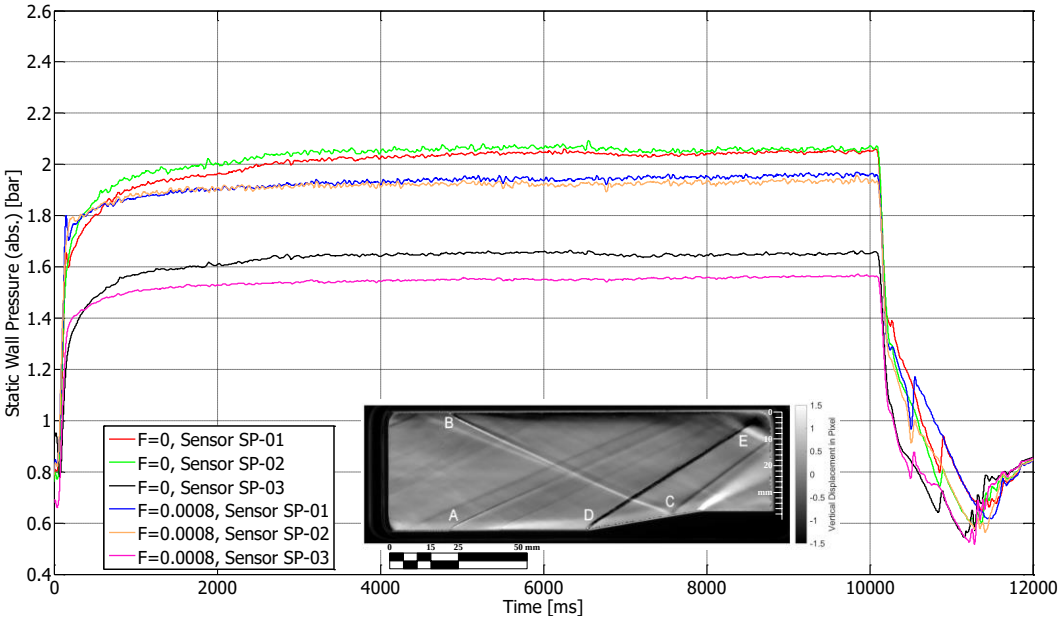

Fig 9. Static Wall Pressures in the Coolant Wake Region, 900 K, 15 bar Stagnation Values, Hydrogen, Shock Generator Position 177 mm, Sika-IL 1.

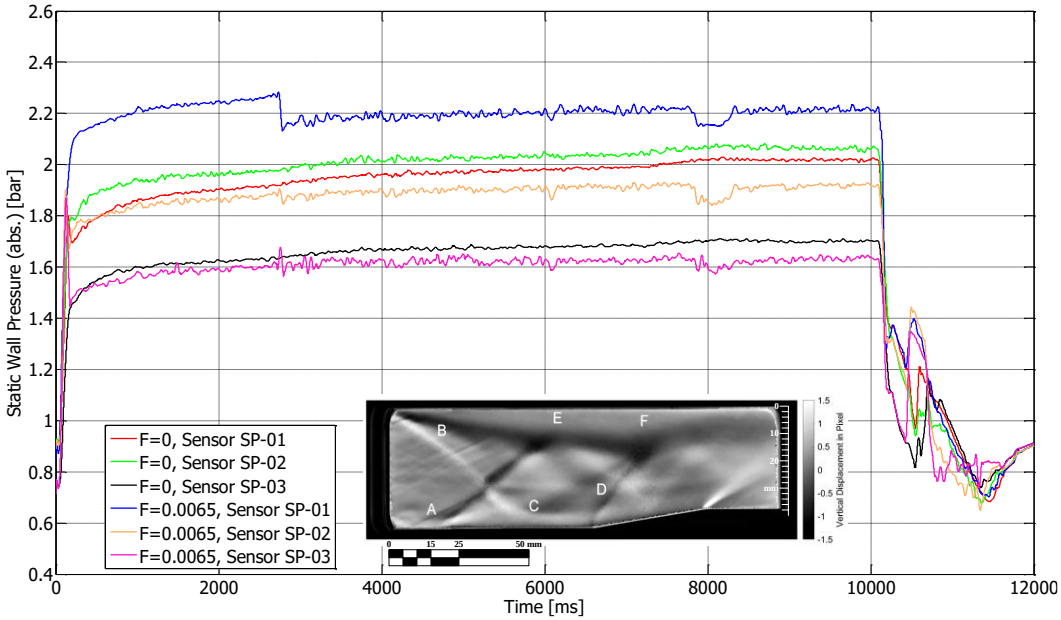

Fig 10. Static Wall Pressures in the Coolant Wake Region, 900 K, 15 bar Stagnation Values, Hydrogen, Shock Generator Position 177 mm, Sika-IL 20.

If the blowing ratio is increased to F=0.65 % (refer to Fig. 10) with Sika-IL 20, a shock train develops. First it shows a nominal flow pattern, but at approximately 3 s into the run, the coolant boundary layer shifts to an upstream position into a region were no porous wall exists. This causes a repositioning of the shock system, which is indicated for example by the pressure drop at sensor "SP-01". The authors assume that a coolant recirculation zone is created by the specific flow pattern at this boundary condition resulting in the upstream movement of the coolant. However, this still needs to be confirmed by the analysis of additional measurement data. At a shock generator position of 112 mm no shock train develops at this blowing ratio (refer to [19]).

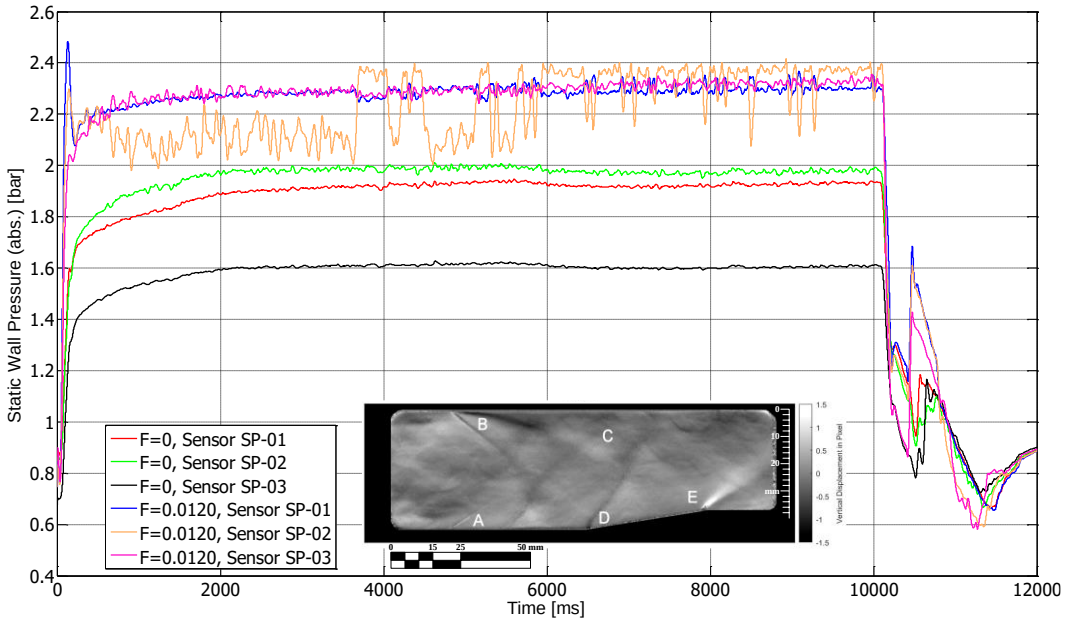

Fig 11. Static Wall Pressures in the Coolant Wake Region, 900 K, 15 bar Stagnation Values, Hydrogen, Shock Generator Position 177 mm, Sika-R 150.

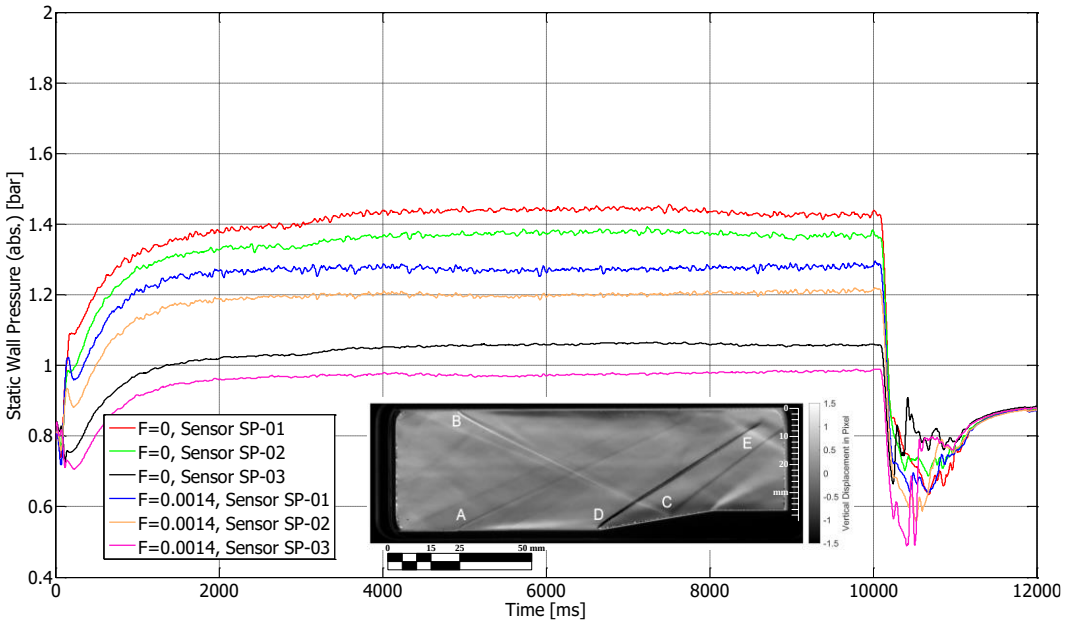

Fig 12. Static Wall Pressures in the Coolant Wake Region, 1200 K, 10 bar Stagnation Values, Hydrogen, Shock Generator Position 177 mm, Sika-IL 1.

If the blowing ratio is increased further to F=1.2 % (see Fig. 11), the flow starts to develop not only a shock train, but is forced close to the fully choked state of Fig. 8. The higher hot gas mass flow rate of the air vitiator in Fig. 11 compared to Fig. 8 forces the flow into a still supersonic state, seen by the pale shock train structures in the BOS image in Fig. 11. This leads to a frequent shock repositioning, which is indicated by the strong wall pressure fluctuations, especially at sensor station "SP-03" in Fig. 11. This boundary condition also developed one of the strongest acoustical emissions in the experiments. Compared to the results of a shock generator position at 112 mm, the maximum wall pressure is approx. 1.0 bar higher in Fig. 11. At this boundary condition the phenomenon of the flipping or shifting shock train (nominal flow to shock train and vice versa) occurred at the 112 mm position (see [19]). For Fig. 12 the air vitiator's boundary conditions have been changed to a 1200 K stagnation temperature and 10 bar stagnation pressure. As in the 900 K, 10 bar and 15 bar cases in Figs. 6 and 9, the wall pressure distribution reacts more strongly and distinctly to the introduction of a coolant secondary flow, than in the 112 mm case (refer to [19]).

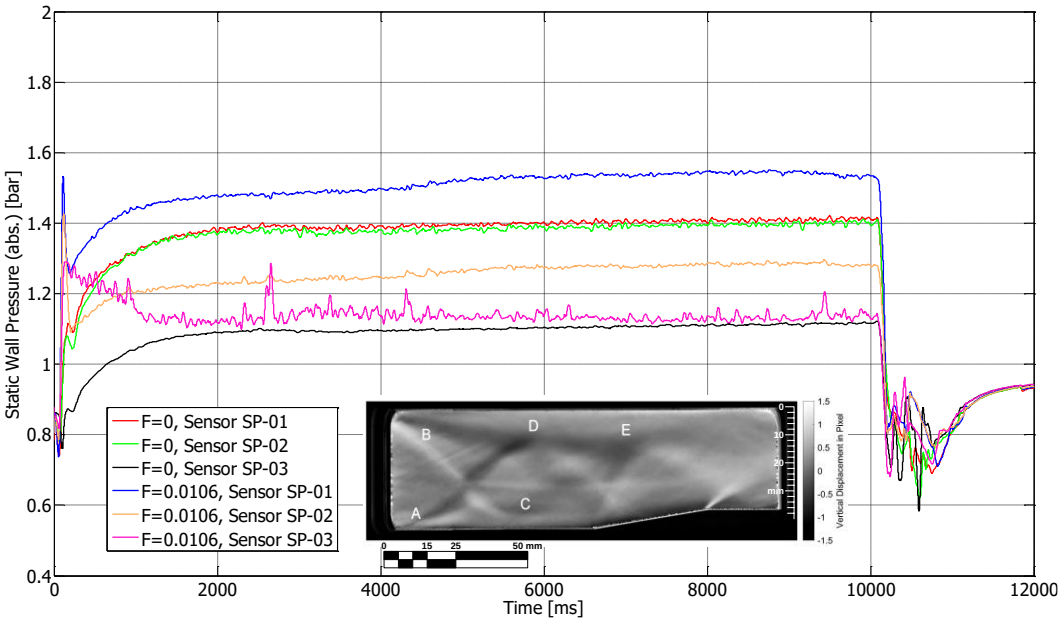

Fig 13. Static Wall Pressures in the Coolant Wake Region, 1200 K, 10 bar Stagnation Values, Hydrogen, Shock Generator Position 177 mm, Sika-IL 20.

Figure 13 displays the static wall pressure distribution at a 1200 K, 10 bar stagnation condition with Sika-IL 20. At this boundary condition a behavior similar to Fig. 10 is visible: the coolant boundary layer starts at the porous wall section, but moves upstream while the shock train system fully develops. This strongly affects the static wall pressure distribution. All sensors show a peak during the first 0.25 to 0.5 seconds runtime.

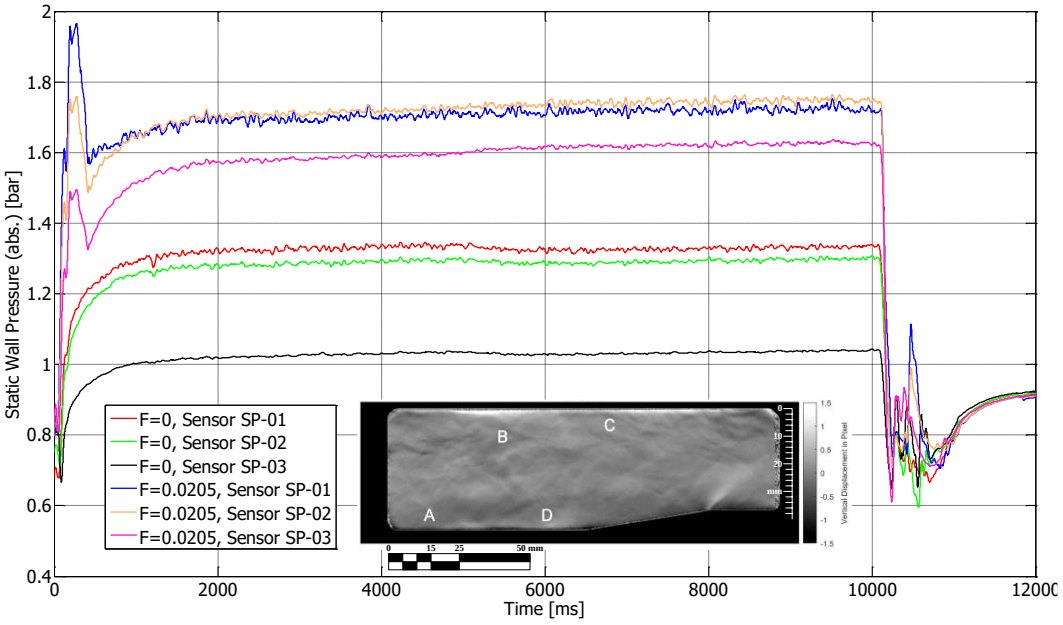

Fig 14. Static Wall Pressures in the Coolant Wake Region, 1200 K, 10 bar Stagnation Values, Hydrogen, Shock Generator Position 177 mm, Sika-R 150.

After that, the reading of sensor "SP-03" starts to drop strongly fluctuating. This corresponds to the BOS snapshot in Fig. 13 and the BOS image analysis in [7]. In [7] the coolant boundary layer behaves nominal up to a blowing ratio of F=0.79 %. At higher blowing ratios it shifts even upstream of the porous section together with an upstream repositioning of the shock train. Figure 14 displays the static wall pressure distribution at a 1200 K, 10 bar stagnation condition with Sika-R 150 at the lowest tested air vitiator mass flow rate. The experiments showed that this boundary condition is most prone to SBLI induced self-ignition of the hydrogen coolant boundary layer. This can be seen in Fig. 14 by the strong

wall pressure peak over all pressure sensors during the first 0.5 to 1.0 seconds of runtime. This self-ignition temporarily chokes the flow field in the model combustion chamber or brings it close to the choking condition. After the flame gets blown out or quenched, the wall pressure distribution returns to nominal values and the supersonic flow continues.

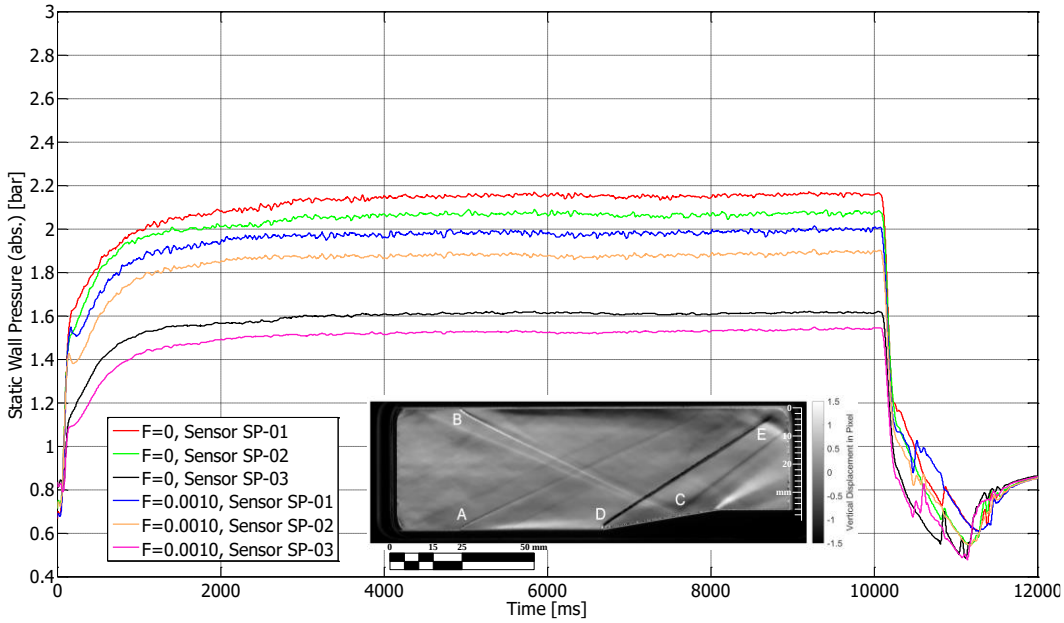

Fig 15. Static Wall Pressures in the Coolant Wake Region, 1200 K, 15 bar Stagnation Values, Hydrogen, Shock Generator Position 177 mm, Sika-IL 1.

In Fig. 15 the wall pressure distribution is displayed for the 1200 K, 15 bar stagnation condition with Sika-IL 1. The pressure distribution shows the same sensitivity to the introduction of a coolant secondary flow as in Fig. 6, Fig. 9, and Fig. 12 and in contrast to [19].

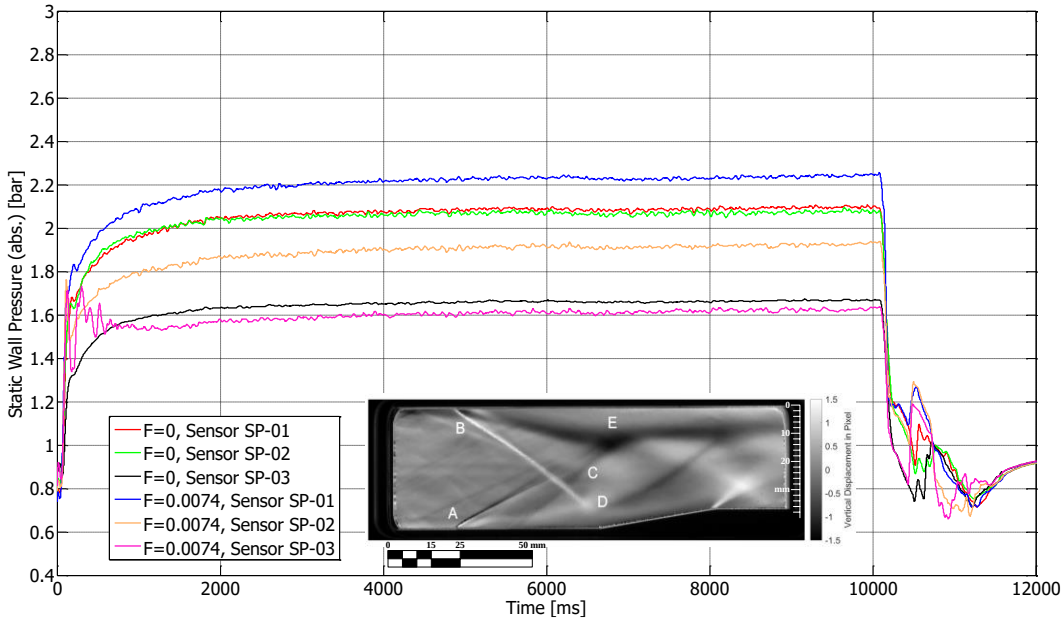

Fig 16. Static Wall Pressures in the Coolant Wake Region, 1200 K, 15 bar Stagnation Values, Hydrogen, Shock Generator Position 177 mm, Sika-IL 20.

In Fig. 16 the coolant boundary layer starts within the first second of the test run with an instability in the behavior, indicated by the pressure jitter at sensor "SP-03" and confirmed by the BOS analysis of [6]. The maximum pressure values are approx. 1.1 bar higher than for the 112 mm shock generator position (refer to [19]). However the flow appears to be more stable at the 177 mm position than at the 112 mm position (refer to [19] for details).

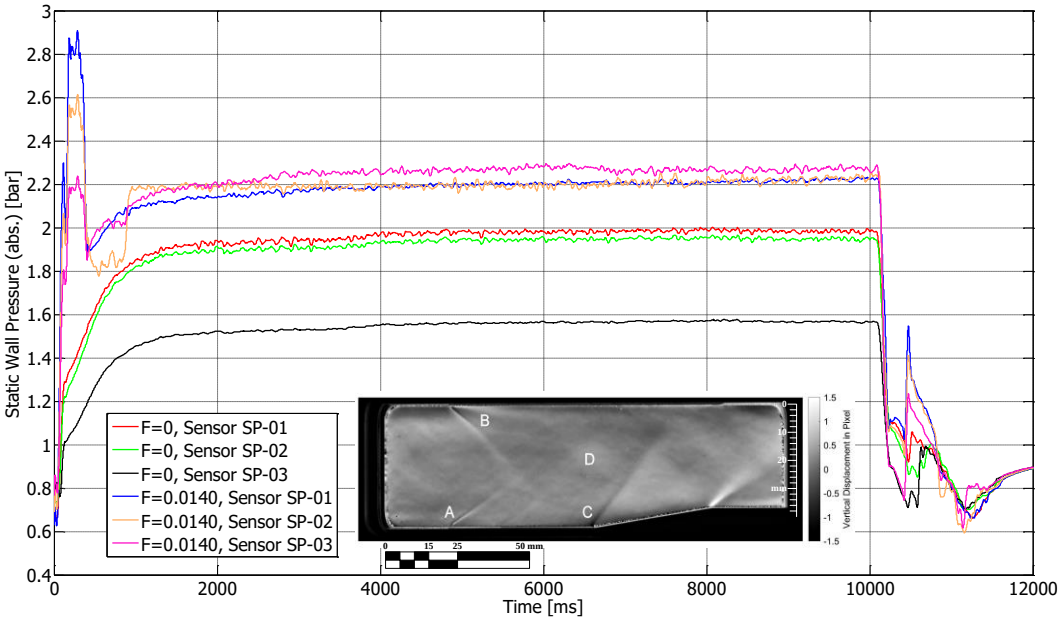

Fig 17. Static Wall Pressures in the Coolant Wake Region, 1200 K, 15 bar Stagnation Values, Hydrogen, Shock Generator Position 177 mm, Sika-R 150.

Figure 17 shows the static wall pressure distribution with Sika-R 150 at a 1200 K stagnation temperature and a 15 bar stagnation pressure. SBLI induced self-ignition of the hydrogen coolant appeared at this testing point (refer to self-ignition analysis in [7]). This is indicated in Fig. 17 by the static wall pressure peaks at all three sensor stations within the first second of the test run. This sudden pressure rise brought the flow close to the choking condition, similar to Fig. 14.

5. Conclusion

The DLR at Lampoldshausen conducted experiments on the applicability of transpiration cooling systems in supersonic combustion ramjets. For this publication gaseous hydrogen was used as coolant together with three different porous wall materials made of sintered stainless steel and a wedge shaped shock generator that was investigated at one horizontal position in the model combustion chamber (177 mm). For all porous samples and each boundary condition of the air vitiator, the static wall pressure distributions at the maximum blowing ratio were analyzed and compared with the uncooled case (no blowing ratio). The analysis was supported by a Background Oriented Schlieren (BOS) image analysis for the different maximum blowing ratios in order to visualize differences and deviations in the flow field. Compared to the case where the shock generator is positioned at 112 mm, even small blowing ratios generated a more distinct pressure distribution in the static wall pressure. If the shock generator is positioned at 177 mm, the greater local thickness of the coolant boundary layer at this position results in a stronger geometric contraction. This indicated a stronger sensitivity of this shock generator position to the development of shock trains compared to the 112 mm position. These shock trains increase the static wall pressure in the coolant wake region and additionally can lead faster to a choked flow condition. If the flow is choked this results in a high pressure rise, possible SBLI induced self-ignition and eventually strong pressure fluctuations. At 112 mm, if the blowing ratio is increased further, the shock reflection point position has an increasingly higher influence on the static wall pressure distribution. The sudden build-up of shock trains or the sudden switch from a nominal flow pattern drastically increases the static wall pressure and further stabilizes this flow pattern. It was proven in this publication that the main drivers for influencing the static wall pressure distribution are the hot gas mass flow rate (stagnation pressure is more important than stagnation temperature) and the impingement position of the shock generator's oblique shock. The static wall pressure distribution was found to be mostly independent of the changes in static wall temperature and in cooling efficiency. However, an exception has to be made for SBLI induced self-ignition cases, because the shock train induced by the ignition and the pressure rise connected with it, improves the mixing of hot gas and coolant secondary flow. This causes a rise in the static wall temperature and eventually leads to a decrease of the cooling efficiency.

6. Outlook

Additional experiments have been performed to determine the effect of different shock generator horizontal positions. A comparison of the static wall pressure distribution for different shock generator positions will be included in future publications. The lateral static wall pressure distribution has been determined for nitrogen and hydrogen as coolants, different porous media and different shock generator positions. The data from these measurements will be discussed in future publications and will help to thoroughly analyze the pressure distribution along the model combustion chamber. This will help to better understand the pressure phenomena shown in this publication as well as shock train and SBLI self-ignition build-up. Further experiments using CMC fiber reinforced ceramics of different thicknesses have been performed using nitrogen and hydrogen as coolant and different shock generator positions. The results of those experiments will be part of future publications by the authors together with an analysis of SBLI related damage mechanisms that were encountered during the CMC test campaign. Results of tests with extended run times and the effect on the temperature and pressure distribution in the setup will be addressed in future publications. Improvements to existing theoretical cooling models are being developed in order to better depict the situation of a temperature measurement in the coolant wake region.

7. Uncertainty Analysis

For every test run of the presented data, the random uncertainty of the mean $P_{\bar{x}}$ was calculated for the blowing ratio using Eq. 2 (see [20]). In Eq. 2, S_x indicates the standard deviation, and n represents the number of measurements used for determining the average.

$$P_{\bar{x}} = 2\frac{S_x}{n^{0.5}} \tag{2}$$

The stagnation pressure is determined via the pressure measurement and the velocity calculation in the air vitiator. The highest random uncertainty of the mean value in the pressure measurement was 0.065 bar for a 15 bar stagnation pressure and 0.040 bar for a 10 bar stagnation pressure. Assuming a systematic uncertainty of the thermocouples of (0.0075*measured temperature value) according to the manufacturer, the maximum total uncertainty for the stagnation temperature measurement is 2.46 K. This causes a calculation uncertainty of about 0.4 % or 2.2 K of the supersonic nozzle exit temperature T_e in the worst case. Thus, the uncertainty of the blowing ratio caused by measurement uncertainties is below 2 %. For the different figures, the random uncertainty of the mean was determined as follows: Fig. 6: 1.022E-3 bar; Fig. 7: 1.233E-3 bar; Fig. 8: 2.175E-3; Fig. 9: 2.753E-3 bar; Fig. 10: 2.973E-3 bar; Fig. 11: 3.240E-3 bar; Fig. 12: 1.310E-3 bar; Fig. 13: 1.379E-3 bar; Fig. 14: 1.937E-3 bar; Fig. 15: 2.969E-3 bar; Fig. 16: 2.986E-3 bar, Fig. 17: 3.148E-3 bar.

References

1. Sholto, F., Smart, M. K., Kearney, M. P., Jahn, I.: Flyback of the SPARTAN Scramjet-Powered Launch Vehicle. AIAA- American Institute of Aeronautics and Astronautics, AIAA 2018-2177 (2018). https://doi.org/10.2514/6.2018-2177
2. Kerst, A., Gross, K. C., Oren, E. P., Komives, J. R., Rhoby, M., Ombrello, T.: Preliminary Investigation of a Scramjet Flowfield with Hyperspectral Imaging. AIAA- American Institute of Aeronautics and Astronautics, AIAA 2017-4646 (2017). https://doi.org/10.2514/6.2017-4646
3. Speier, R., Nacouzi, G., Lee, C., Moore, R.: Hypersonic Missile Nonproliferation - Hindering the Spread of a New Class of Weapons. RAND Corporation, RR-2237-CC (2017). https://doi.org/10.7249/RR2137
4. Langener, T., von Wolfersdorf, J.; Kuhn, M., Steelant, J.: Transpiration cooling with supersonic flows and foreign gas injection. AIAA- American Institute of Aeronautics and Astronautics, AIAA 2010-6794 (2010). https://doi.org/10.2514/6.2010-6794
5. Langener, T.: A Contribution to Transpiration Cooling for Aerospace Applications Using CMC Walls. PhD thesis, University of Stuttgart, Germany (2011).

6. Greuel, D.: Untersuchungen zum Impuls- und Stofftransport in effusive gekühlten faserkeramischen Brennkammerwänden (Investigations on Momentum and Mass Transport in Effusion Cooled Rocket Combustion Chambers Made of Fibre Ceramics). PhD thesis, RWTH Aachen, Germany (2013).
7. Strauss, F., General, S., Manfletti, C., Schlechtriem, S.: Flow Path and Interaction Analysis in a Hydrogen Transpiration Cooled Scramjet Model Combustor. AIAA- American Institute of Aeronautics and Astronautics, AIAA 2019-4015, (2019). https://doi.org/10.2514/6.2019-4015
8. Strauss, F., General, S., Manfletti, C., Schlechtriem, S.: Flow Visualizations with Background Oriented Schlieren in a Transpiration-Cooled Model Scramjet Combustor. Int. J. of Energetic Mat. and Chem. Prop. 18(2), 133-155 (2019). https://doi.org/10.1615/IntJEnergeticMaterialsChemProp.2019028003
9. Strauss, F., Manfletti, C., Lieberwirth, R. and Schlechtriem, S., "Experimental Setup on Transpiration Cooling in Supersonic Combustion Ramjets (Scramjets)," 5th Space Propulsion Conference, 2nd to 6th May 2016, Rome, Italy, (2016).
10. Strauss, F., Manfletti, C., Freudenmann, D., Witte, J., Schlechtriem, S.: Preliminary Experiments on Transpiration Cooling in Ramjets and Scramjets. AIAA- American Institute of Aeronautics and Astronautics, AIAA 2016-4968, (2016). https://doi.org/10.2514/6.2016-4968
11. Strauss, F., Woessner, M., Weisswange, M., Manfletti, C., Schlechtriem, S.: Experiments on Flow Interaction in a Transpiration Cooled Model Scramjet. 7th European Conference of Aeronautics and Space Sciences (EUCASS), 3rd to 6th July, 2017, Milan, Italy. EUCASS 2017-235, (2017). https://doi.org/10.13009/EUCASS2017-235
12. Strauss, F., Witte, J., Weisswange, M., Manfletti, C., Schlechtriem, S.: Experiments on Shock-Boundary Layer Interaction and Cooling Efficiency in a Transpiration Cooled Model Scramjet. AIAA- American Institute of Aeronautics and Astronautics, AIAA 2017-4833, (2017). https://doi.org/10.2514/6.2017-4833
13. Strauss, F., Witte, J., Manfletti, C., Schlechtriem, S.: Experiments on Nitrogen and Hydrogen Transpiration Cooling in Supersonic Combustion Ramjets (Scramjets). 6th Space Propulsion Conference, 14th to 18th May 2018, Seville, Spain (2018).
14. Strauss, F., Witte, J., General, S., Manfletti, C., Schlechtriem, S.: Experiments on Nitrogen and Hydrogen Transpiration Cooling in a Model Scramjet Combustor. AIAA- American Institute of Aeronautics and Astronautics, AIAA 2018-4932 (2018). https://doi.org/10.2514/6.2018-4932
15. Strauss, F., General, S., Manfletti, C., Schlechtriem, S.: Experimental Flow Path Analysis of a Hydrogen Transpiration Cooled Model Scamjet Combustor. 8th European Conference for Aeronautics and Space Sciences (EUCASS), 1st to 5th July 2019, Madrid, Spain (2019). https://doi.org/10.13009/EUCASS2019-516
16. Settles, G. S.: Schlieren and Shadowgraph Techniques. 1st ed., Springer, Heidelberg (2001)
17. Settles, G. S., Hargather, M.: A Review of Recent Developments in Schlieren and Shadowgraph Techniques. Meas. Science and Techn. 28, 042001, (2017). https://doi.org/10.1088/1361-6501/aa5748
18. Babinsky, H., Harvey, J. K.: Shock Wave-Boundary-Layer Interactions. 1st ed., Cambridge University Press, New York (2011)
19. Strauss, F., General, S., Cragg, P., Schlechtriem, S.: Wall Pressure Effects and Shock-Boundary Layer Interactions in a Transpiration Cooled Scramjet Model Combustor, 23rd AIAA International Space Planes and Hypersonic Systems and Technologies Conference, 10th to 12th March 2020, Montréal, Canada, AIAA 2020-2438 (2020). https://doi.org/10.2514/6.2020-2438
20. Wheeler, J., Ganji, A.: Introduction to Engineering Experimentation, 3rd ed., Pearson (2010)